

ViSurf: Visual Supervised-and-Reinforcement Fine-Tuning for Large Vision-and-Language Models

Yuqi Liu¹ Liangyu Chen³ Jiazen Liu² Mingkang Zhu¹ Zhisheng Zhong¹ Bei Yu¹ Jiaya Jia²
 CUHK¹ HKUST² RUC³

Abstract

Typical post-training paradigms for Large Vision-and-Language Models (LVLMs) include Supervised Fine-Tuning (SFT) and Reinforcement Learning with Verifiable Rewards (RLVR). SFT leverages external guidance to inject new knowledge, whereas RLVR utilizes internal reinforcement to enhance reasoning capabilities and overall performance. However, our analysis reveals that SFT often leads to sub-optimal performance, while RLVR struggles with tasks that exceed the model’s internal knowledge base. To address these limitations, we propose ViSurf (Visual Supervised-and-Reinforcement Fine-Tuning), a unified post-training paradigm that integrates the strengths of both SFT and RLVR within a single stage. We analyze the derivation of the SFT and RLVR objectives to establish the ViSurf objective, providing a unified perspective on these two paradigms. The core of ViSurf involves injecting ground-truth labels into the RLVR rollouts, thereby providing simultaneous external supervision and internal reinforcement. Furthermore, we introduce three novel reward control strategies to stabilize and optimize the training process. Extensive experiments across several diverse benchmarks demonstrate the effectiveness of ViSurf, outperforming both SFT, RLVR, and two-stage SFT → RLVR. In-depth analysis corroborates these findings, validating the derivation and design principles of ViSurf. The code will be publicly available.

1. Introduction

Developing Large Vision-and-Language Models (LVLMs) that excel in diverse visual perception tasks is a promising direction for visual intelligence. To this end, prior work has predominantly relied on two training paradigms: Supervised Fine-Tuning (SFT) [1, 17, 38] and Reinforcement Learning with Verifiable Rewards (RLVR) [20, 21].

Every coin has two sides, and these paradigms are no exception. SFT directly optimizes the model using expert-annotated data. This approach provides explicit external guidance, enabling the model to memorize the target distribution. However, it often exhibits sub-optimal performance

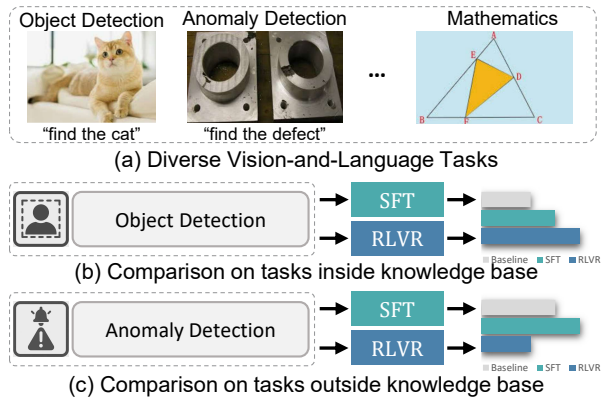


Figure 1. (a) Examples of vision-and-language tasks. (b) For tasks within LVLMs’ knowledge base, RLVR performs better than SFT. (c) For tasks that exceed LVLMs’ knowledge base, SFT performs better, whereas RLVR performs worse than baseline.

and can lead to catastrophic forgetting of pre-trained knowledge. Recently, RLVR has garnered significant research attention. The on-policy RLVR methods start with an initial policy and iteratively generates a group of rollouts that are evaluated by pre-defined reward functions, then the policy is subsequently optimized based on this internal feedback, such as Group Relative Policy Optimization (GRPO) [34] and Dynamic Sampling Policy Optimization (DAPO) [42]. By leveraging internal reinforcement signals, RLVR mitigates catastrophic forgetting and often achieves superior performance. Nevertheless, its performance can degrade when tasks extend beyond the initial model’s knowledge base. We evaluate these two paradigms across a diverse set of vision-and-language tasks, with our key findings summarized in Figure 1. The results indicate that SFT is more effective for tasks that fall outside the pre-training distribution of LVLMs, whereas RLVR yields superior performance on tasks that align with its pre-existing knowledge base. We also provide a case study in Section 3.2 to illustrate this phenomenon. Although a sequential SFT → RLVR pipeline tries to leverage their complementary strengths, this two-stage method incurs the combined computational cost of

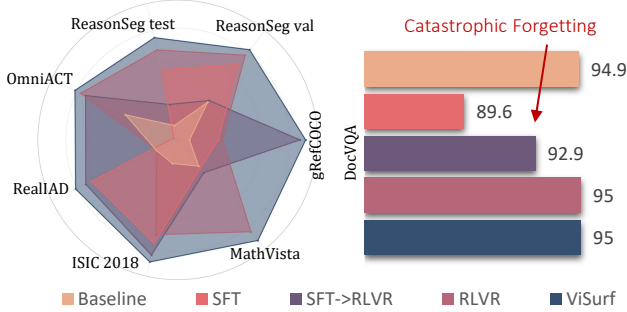


Figure 2. Radar Chart: ViSurf achieves superior performance across different training paradigms. Bar Chart: SFT and two-stage SFT → RLVR exhibit catastrophic forgetting.

both stages and remains susceptible to catastrophic forgetting during the initial SFT phase.

To address the aforementioned limitations, we propose ViSurf (Visual Supervised-and-Reinforcement Fine-Tuning), a unified, single-stage post-training paradigm designed to integrate the complementary advantages of SFT and RLVR. We begin with an analysis of the underlying objectives and gradients of SFT and RLVR. We theoretically demonstrate that their gradients share similar patterns, enabling them to be integrated into a single, unified objective, the ViSurf objective. Unlike prior methods [25, 43] that combine SFT and RLVR through simple objective addition, ViSurf offers a unified perspective for these two training paradigms. While subtle differences exist, the gradient of ViSurf objective can be interpreted as a composite of the gradients from both SFT and RLVR. Based on the theoretical analysis, we design three reward control strategies to stabilize training. Specifically, for the ground-truth labels, we i) aligning them with rollouts preference, ii) eliminating thinking reward for them, and iii) smoothing the reward for them. The implementation of ViSurf is consequently simplified to interleaving ground-truth demonstrations with on-policy rollouts in a unified training phase.

We conduct extensive experiments across various domains, with a comparative summary presented in Figure 2. The results indicate that our method, ViSurf, achieves superior performance than SFT, RLVR and SFT → RLVR. Models trained with ViSurf also exhibit reasoning abilities similar to those established in previous works [20, 21]. Furthermore, ViSurf successfully mitigates catastrophic forgetting, as evidenced by its stable performance on VQA tasks. The ablation study confirms the critical contribution of the proposed reward control mechanism. Additional in-depth analysis provides empirical validation for our theoretical analysis and offers insights into the operational principles of ViSurf. Our contributions are summarized as follows:

- Based on our theoretical analysis, we propose ViSurf, a unified post-training paradigm that leverages the comple-

mentary benefits of SFT and RLVR.

- We design three reward control strategies to stabilize the training process, the necessity of which is validated through ablation studies.
- Empirically, ViSurf outperforms existing post-training methods (SFT, RLVR, and SFT → RLVR). Additional analyses offer a thorough understanding of its mechanics.

2. Related Works

2.1. Supervised Fine-tuning for LVLMs

Supervised Fine-Tuning (SFT) is a predominant paradigm for training Large Vision-Language Models (LVLMs). This approach involves fine-tuning pre-trained models on expert-annotated data. The pioneering work in this area is LLaVA [17], which has inspired numerous subsequent models. Notable examples include the LLaVA-series [13, 18], QwenVL-series [1, 38], MGM-series [14, 36, 44], and InternVL [3], all of which adopt this paradigm. SFT has proven particularly effective for adapting LVLMs to diverse downstream applications, such as image quality assessment [41], visual counting [5], and autonomous driving [40].

2.2. Reinforcement Learning for LVLMs

Reinforcement Learning (RL) is a standard method for fine-tuning Large Vision-Language Models (LVLMs). Among RL algorithms, Direct Preference Optimization (DPO) [30] relies on pre-collected human preference datasets, which can be costly to produce. Similarly, Proximal Policy Optimization (PPO) [32] requires a well-trained reward model to evaluate responses generated by the policy. Recently, RLVR algorithms, such as GRPO [34] and DAPO [42], have gained attention for their ability to assess model outputs against objective criteria. This approach reduces the dependency on manually annotated data and pre-trained reward models. The effectiveness of RLVR for LVLMs has been demonstrated in recent works [9, 19–22] such as SegZero [20] and VisualRFT [22].

3. ViSurf

We begin by analyzing the objective functions of SFT and RLVR in Section 3.1. A case study in Section 3.2 then highlights the limitations of both methods. To address these limitations, we introduce ViSurf, detailing its design and relationship to SFT and RLVR in Section 3.3. Subsequently, Section 3.4 presents three novel mechanisms for reward control during training, and Section 3.5 provides an analysis of the optimization process.

3.1. Preliminary

Let π_θ denote a large vision-and-language model (LVLM), parameterized by θ . Common post-training paradigms for optimizing π_θ include Supervised Fine-Tuning (SFT) and

Reinforcement Learning with Verifiable Rewards (RLVR). Both SFT and RLVR utilize the same input dataset, $\mathcal{D}_{\text{input}} = \{(v_i, t_i)\}_{i=1}^N$, where v_i is a visual input, t_i is a textual input, and N is the dataset size.

Supervised Fine-Tuning (SFT) optimizes π_θ against a set of ground-truth labels, $\mathcal{D}_{\text{label}} = \{y_i\}_{i=1}^N$. The objective is to minimize the negative log-likelihood of the labels:

$$\mathcal{L}_{\text{SFT}}(\theta) = -\mathbb{E}_{\substack{(v, t) \sim \mathcal{D}_{\text{input}} \\ y \sim \mathcal{D}_{\text{label}}}} [\log \pi_\theta(y | v, t)], \quad (1)$$

where y corresponds to (v, t) . A more precise notation would be $(v, t, y) \sim \text{zip}(\mathcal{D}_{\text{input}}, \mathcal{D}_{\text{label}})$. Nevertheless, we retain the current notation, $(v, t) \sim \mathcal{D}_{\text{input}}, y \sim \mathcal{D}_{\text{label}}$, for clarity and ease of comparison in the subsequent discussion.

Reinforcement Learning with Verifiable Rewards (RLVR). We illustrate RLVR using the on-policy Group Relative Policy Optimization (GRPO) algorithm [34]. GRPO optimizes the policy π_θ using a verifiable reward function, which typically combines measures of output format and accuracy [7, 20, 21]. For a given input $(v_i, t_i) \in \mathcal{D}_{\text{input}}$, the old policy $\pi_{\theta_{\text{old}}}$ (from a previous optimization step) generates a group of G rollouts $\{o_j\}_{j=1}^G$ by sampling with different random seeds. Each rollout o_j is then evaluated by a reward function $r(\cdot)$, resulting in a set of rewards $\{r(o_j)\}_{j=1}^G$. The advantage for each rollout is subsequently computed as follows:

$$\hat{A}_j = \frac{r(o_j) - \text{mean}(\{r(o_j)\}_{j=1}^G)}{\text{std}(\{r(o_j)\}_{j=1}^G)}, \quad (2)$$

The objective of RLVR is to minimize the equation:

$$\mathcal{L}_{\text{RLVR}}(\theta) = -\mathbb{E}_{\substack{(v, t) \sim \mathcal{D}_{\text{input}} \\ \{o_j\}_{j=1}^G \sim \pi_{\theta_{\text{old}}}}} \left[\frac{1}{G} \sum_{j=1}^G \min \left\{ \frac{\pi_\theta(o_j | v, t)}{\pi_{\theta_{\text{old}}}(o_j | v, t)} \hat{A}_j, \text{clip} \left(\frac{\pi_\theta(o_j | v, t)}{\pi_{\theta_{\text{old}}}(o_j | v, t)}, 1 - \epsilon, 1 + \epsilon \right) \hat{A}_j \right\} \right], \quad (3)$$

where the ϵ is a constant that controls the clipping boundary. For simplicity, both in equation and in our practical implementation, we omit the KL divergence term.

3.2. Case Study: Non-Object Scenarios

We present a case study on non-object referring expression segmentation. In this task, instructions comprise both correct expressions (referring to existing objects) and incorrect ones (where the referred objects are absent). For this study, we utilize the VisionReasoner model [21], which is initialized with Qwen2.5VL [1] and SAM2 [31] and has demonstrated strong performance on standard referring segmentation tasks. Figure 3(a) illustrates the non-object segmentation and the architecture of VisionReasoner. Detailed experimental settings are demonstrated Section 4.1.

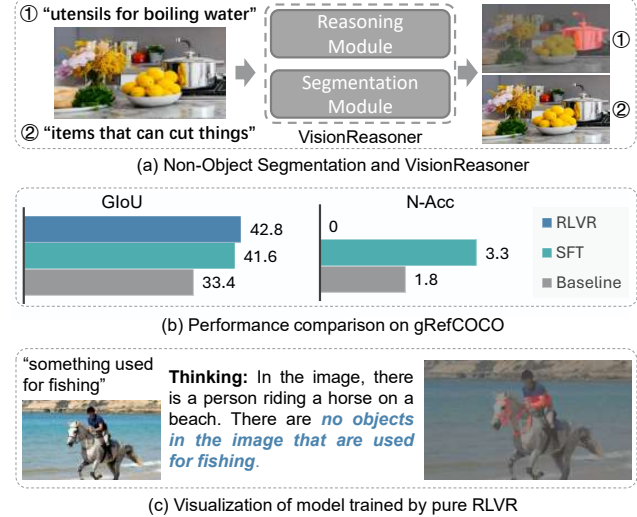


Figure 3. (a) Illustration on Non-Object Segmentation and VisionReasoner. (b) Performance comparison of SFT and RLVR on gRefCOCO. While RLVR achieves higher overall GIoU, it fails on non-object instructions. (c) Specifically, the RLVR model consistently outputs a mask even when no relevant object is detected.

The gRefCOCO [16] serves as the benchmark for this scenario. We compare gIoU (average IoU across images) and N-Acc (accuracy in identifying non-existent object). Quantitative and qualitative results are presented in Figure 3(b)-(c). Our analysis reveals that model trained by SFT achieves suboptimal gIoU performance but tends to learn to correctly identify the absence of objects. In contrast, model trained with RLVR exhibits a more coherent reasoning process and attain higher overall gIoU scores, yet they often generate object masks even when no relevant object is present. This limitation arises because the RLVR model, relying solely on self-rollouts, lacks the corrective mechanism necessary to produce a “no object” output. In essence, RLVR enhances overall performance through internal self-guidance, whereas SFT provides crucial external guidance when self-rollouts fail. This analysis leads to a key question: *how can we integrate the benefits of both training paradigms in a single training stage efficiently?*

3.3. Combining SFT and RLVR

To harness the complementary benefits of SFT and RLVR, we propose ViSurf: a unified, single-stage post-training algorithm. This section elaborates on the derivation of the ViSurf algorithm and its relation to SFT and RLVR.

Gradient Analysis of SFT and RLVR. The gradient of SFT can be derived from Equation (1) as:

$$\nabla_\theta \mathcal{L}_{\text{SFT}}(\theta) = -\mathbb{E}_{\substack{(v, t) \sim \mathcal{D}_{\text{input}} \\ y \sim \mathcal{D}_{\text{label}}}} [\nabla_\theta \log \pi_\theta(y | v, t)]. \quad (4)$$

The gradient of RLVR can be derived from Equation (3)

using approximation $\pi_\theta \approx \pi_{\theta_{old}}$ and log-derivative trick. We also omit clip operation for simplicity:

$$\begin{aligned} \nabla_\theta \mathcal{L}_{RLVR}(\theta) &= -\mathbb{E}_{\substack{(v,t) \sim \mathcal{D}_{input} \\ \{o_j\}_{j=1}^G \sim \pi_{\theta_{old}}}} \\ &\quad \left[\frac{1}{G} \sum_{j=1}^G \hat{A}_j \nabla_\theta \log \pi_\theta(o_j | v, t) \right]_{\theta \approx \theta_{old}}. \end{aligned} \quad (5)$$

We observe that the gradients of the SFT and RLVR losses, $\nabla_\theta \mathcal{L}_{SFT}(\theta)$ and $\nabla_\theta \mathcal{L}_{RLVR}(\theta)$, share a similar form. The difference between them is the guidance signal (y vs. $\{o_j\}_{j=1}^G$) and coefficient (1 vs. \hat{A}_j).

Objective of ViSurf. To combine SFT and RLVR into a single stage, we design an objective function that naturally yields a gradient combining both $\nabla_\theta \mathcal{L}_{SFT}(\theta)$ and $\nabla_\theta \mathcal{L}_{RLVR}(\theta)$. Our key insight is to include the ground-truth label y as a high-reward sample within the RLVR framework. We construct an augmented rollout set $y \cup \{o_j\}_{j=1}^G$. Then the corresponding rewards are $r(y) \cup \{r(o_j)\}_{j=1}^G$. This formulation modifies the advantage calculation of rollouts in Equation (2) as follows:

$$\hat{A}_j = \frac{r(o_j) - \text{mean}(\{r(y) \cup \{r(o_j)\}_{j=1}^G\})}{\text{std}(\{r(y) \cup \{r(o_j)\}_{j=1}^G\})}, \quad (6)$$

and the advantage of ground-truth y is calculated as:

$$\hat{A}_y = \frac{r(y) - \text{mean}(\{r(y) \cup \{r(o_j)\}_{j=1}^G\})}{\text{std}(\{r(y) \cup \{r(o_j)\}_{j=1}^G\})}. \quad (7)$$

The objective of ViSurf is to minimize the equation:

$$\begin{aligned} \mathcal{L}_{ViSurf}(\theta) &= -\mathbb{E}_{\substack{(v,t) \sim \mathcal{D}_{input} \\ \{o_j\}_{j=1}^G \sim \pi_{\theta_{old}} \\ y \sim \mathcal{D}_{label}}} \\ &\quad \left[\frac{1}{G+1} \left(\sum_{j=1}^G \min \left\{ \frac{\pi_\theta(o_j | v, t)}{\pi_{\theta_{old}}(o_j | v, t)} \hat{A}_j, \right. \right. \right. \\ &\quad \left. \left. \left. \text{clip} \left(\frac{\pi_\theta(o_j | v, t)}{\pi_{\theta_{old}}(o_j | v, t)}, 1 - \epsilon, 1 + \epsilon \right) \hat{A}_j \right\} \right. \right. \\ &\quad \left. \left. + \min \left\{ \frac{\pi_\theta(y | v, t)}{\pi_{\theta_{old}}(y | v, t)} \hat{A}_y, \right. \right. \right. \\ &\quad \left. \left. \left. \text{clip} \left(\frac{\pi_\theta(y | v, t)}{\pi_{\theta_{old}}(y | v, t)}, 1 - \epsilon, 1 + \epsilon \right) \hat{A}_y \right\} \right) \right]. \end{aligned} \quad (8)$$

With the objective function demonstrated above, the pseudocode of ViSurf Optimization Step is shown in Algorithm 1.

Gradient Analysis of ViSurf. The gradient of Equation (8) can be derived using approximation $\pi_\theta \approx \pi_{\theta_{old}}$ and log-derivative trick. We omit clip operation for simplicity:

Algorithm 1: ViSurf Optimization Step

Input: policy model π_θ ; reward function $r(\cdot)$; input data \mathcal{D}_{input} ; label data \mathcal{D}_{label}

for $step = 1, \dots, M$ **do**

- Sample a mini-batch \mathcal{B}_{input} and corresponding \mathcal{B}_{label} ;
- Update the old policy model $\pi_{\theta_{old}} \leftarrow \pi_\theta$;
- Sample G outputs $\{o_j\}_{j=1}^G \sim \pi_{\theta_{old}}(\cdot)$ for each $(v, t) \in \mathcal{B}_{input}$;
- Compute rewards $\{r(o_j)\}_{j=1}^G$ for each sampled output o_j ;
- Compute rewards $r(y)$ for label $y \in \mathcal{B}_{label}$;
- Compute \hat{A}_j and \hat{A}_y through relative advantage estimation;
- Update the policy model π_θ using Equation (8);

Output: π_θ

$$\begin{aligned} \nabla_\theta \mathcal{L}_{ViSurf}(\theta) &= -\mathbb{E}_{\substack{(v,t) \sim \mathcal{D}_{input} \\ \{o_j\}_{j=1}^G \sim \pi_{\theta_{old}} \\ y \sim \mathcal{D}_{label}}} \\ &\quad \left[\frac{1}{G+1} \left(\sum_{j=1}^G \hat{A}_j \nabla_\theta \log \pi_\theta(o_j | v, t) \right. \right. \\ &\quad \left. \left. + \hat{A}_y \nabla_\theta \log \pi_\theta(y | v, t) \right) \right]_{\theta \approx \theta_{old}}. \end{aligned} \quad (9)$$

Relation to SFT and RLVR. We analyze the gradients of ViSurf, SFT, and RLVR to explain their connections. To better illustrate the structure of the gradient, we reformulate Equation (9) as following:

$$\begin{aligned} \nabla_\theta \mathcal{L}_{ViSurf}(\theta) &= \\ &\quad \underbrace{-\mathbb{E}_{\substack{(v,t) \sim \mathcal{D}_{input} \\ \{o_j\}_{j=1}^G \sim \pi_{\theta_{old}}}} \left[\frac{1}{G+1} \sum_{j=1}^G \hat{A}_j \nabla_\theta \log \pi_\theta(o_j | v, t) \right]_{\theta \approx \theta_{old}}}_{\text{RLVR Term}} \\ &\quad \underbrace{-\mathbb{E}_{\substack{(v,t) \sim \mathcal{D}_{input} \\ y \sim \mathcal{D}_{label}}} \left[\frac{1}{G+1} \hat{A}_y \nabla_\theta \log \pi_\theta(y | v, t) \right]_{\theta \approx \theta_{old}}}_{\text{SFT Term}}. \end{aligned} \quad (10)$$

The RLVR term in Equation (10) is structurally identical to the standard RLVR gradient in Equation (5), differing only in its scaling coefficient ($\frac{1}{G+1} \hat{A}_j$ vs. $\frac{1}{G} \hat{A}_j$). Similarly, the SFT term in Equation (10) resembles the SFT gradient from Equation (4), with two key distinctions: (i) the coefficient is weighted by $\frac{1}{G+1} \hat{A}_y$ instead of 1, and (ii) the use of the approximation $\pi_\theta \approx \pi_{\theta_{old}}$. This approximation implies that the ground-truth label y should align with the model's internal generative preference to be effective. Crucially, Equation (9) integrates both the external guidance from SFT and the internal guidance from RLVR.

3.4. Reward Control for Ground-Truth Label

The advantage \hat{A}_y for the ground-truth label y is always positive till now, as the label is correct and receives higher reward, which can lead to reward hacking. The setup is

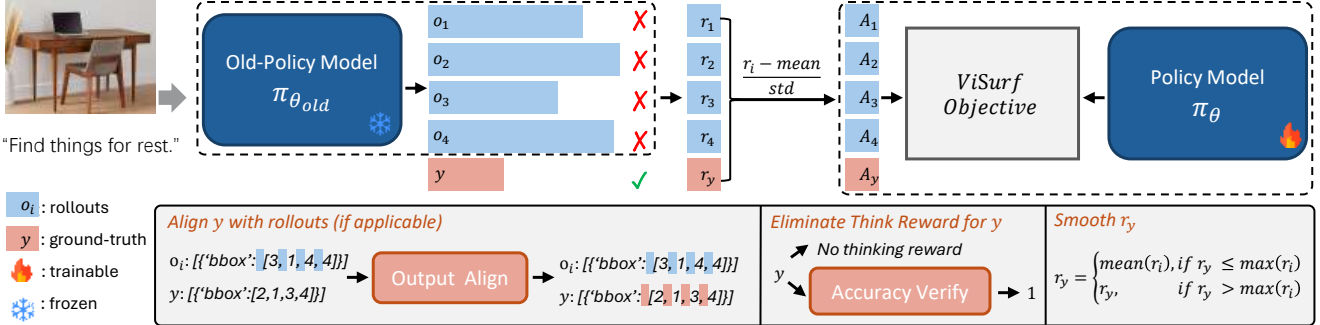


Figure 4. ViSurf Framework. Upper: The integration of external guidance y with internal guidance o_i , which is critical when self-rollouts are unsuccessful. Bottom: Three reward control strategies designed to regulate y , thereby preventing entropy collapse.

sub-optimal for two reasons: (i) the ground-truth lacks a reasoning trace, and (ii) it suppresses the relative advantage \hat{A}_j even if rollouts have already generated correct trace and answer. Furthermore, as analysis above, we must ensure the ground-truth aligns with the self-rollouts to satisfy the approximation $\pi_{\theta} \approx \pi_{\theta_{old}}$. To address these issues, we propose three reward control strategies.

Aligning Ground-truth Labels with Rollouts Preference. To ensure compatibility between the ground-truth data and the self-rollouts generated by π_{θ} , we reformat the ground-truth annotations to match the model’s preferred output style. For instance, we adjust the whitespace in JSON-like structures from $\{\text{'bbox'}:[x1,y1,x2,y2]\}$ to $\{\text{'bbox'}:[x1, y1, x2, y2]\}$ (i.e., adding space after the punctuation), as these variants yield different tokenizations. This alignment minimizes the distribution shift between π_{θ} and $\pi_{\theta_{old}}$, satisfying the underlying assumption $\pi_{\theta} \approx \pi_{\theta_{old}}$.

Eliminating Thinking Reward for Ground-truth Labels. Since the ground-truth labels lack annotated reasoning path, we assign a reasoning format score of zero to them. This operation ensures the model learns reasoning trace directly from its self-rollouts without being biased by missing external reasoning annotations.

Smoothing the Reward for Ground-truth Labels. Prior to advantage estimation, we compare the maximum reward among generated rollouts, $\max\{\{r(o_j)\}_{j=1}^G\}$, against the ground-truth reward $r(y)$. If $\max\{\{r(o_j)\}_{j=1}^G\} \geq r(y)$, it indicates the policy model π_{θ} has already produced a high-quality output without external guidance. In this case, we set $r(y) = \text{mean}\{\{r(o_j)\}_{j=1}^G\}$. This smoothing ensures that the advantage for the ground-truth, \hat{A}_y , becomes zero (as per Equation (7)), eliminating the external supervision signal when it is unnecessary.

3.5. Optimization Analysis During Training

Building on the reward control strategy in Section 3.4, we analyze the dynamics of the terms in Equation (10) throughout training. As defined by Equations (6) and (7), the advan-

tages \hat{A}_j (for rollouts) and \hat{A}_y (for the ground-truth) govern the balance between the RLVR and SFT terms. This balance is self-adaptive. When the policy fails to generate high-quality rollouts, \hat{A}_j decreases (potentially becoming negative), while \hat{A}_y remains high. Consequently, the SFT term dominates the policy update, providing strong external guidance from the ground-truth label. Conversely, when the policy successfully generates desirable rollouts, our reward control mechanism sets $\hat{A}_y \approx 0$, causing the optimization to be dominated entirely by the RLVR term. This automatic shifting between learning modes is a core feature of the single-stage ViSurf paradigm.

Upper Bound Analysis. As mentioned above, our ViSurf is particularly beneficial when old policy model $\pi_{\theta_{old}}$ cannot generate correct rollouts. When the old policy model $\pi_{\theta_{old}}$ already achieves desirable rollouts, the SFT Term in Equation (10) near to zero, thus the upper bound of ViSurf is the RLVR. However, when the policy model cannot generate desirable rollouts, the upper bound is better than using either SFT or RLVR alone.

4. Experiments

Section 4.1 details the experimental settings. We validate ViSurf across diverse domains in Section 4.2, followed by an ablation of the reward control design in Section 4.3. Finally, Section 4.4 provides a in-depth analysis of ViSurf.

4.1. Experimental Settings

We verify ViSurf on benchmarks across several domains.

Non-Object Segmentation. The gRefCOCO [16] includes queries that do not contain corresponding objects. The evaluation metrics are gIoU and N-Acc. We use Multi-objects-7K plus with 200 non-object data for training.

Reasoning Segmentation. The ReasonSeg [12] includes test samples that need reasoning for correct segmentation. It has 200 validation images and 779 test images. The evaluation metric is gIoU. We use Multi-objects-7K proposed in VisionReasoner [21] for training.

Table 1. Comparison on different benchmarks in different domains under different training paradigms.

Method	Non-Object gRefCOCO val		Segmentation ReasonSeg val test		GUI OmniACT test	Anomaly RealIAD subset	Medical:Skin ISIC2018 test	Math MathVista test-mini	Avg
	gIoU	N-Acc	gIoU	gIoU					
Baseline	33.4	1.8	56.9	52.1	60.4	50.1	78.8	68.2	50.2
SFT	41.6	3.3	63.8	60.3	55.4	65.5	91.7	68.3	56.2
RLVR	42.8	0.0	66.0	63.2	65.5	50.0	90.3	71.2	56.1
SFT → RLVR	65.0	52.1	57.2	55.2	64.5	66.9	93.6	68.5	65.4
ViSurf	66.6	57.1	66.5	65.0	65.6	69.3	94.7	71.6	69.6

Table 2. Comparison on VQA under different training paradigms.

Method	ChartQA	DocVQA_val
Baseline	83.8	94.9
SFT	80.8	89.6
RLVR	86.7	95.0
SFT → RLVR	85.0	92.9
ViSurf	87.4	95.0

GUI Grounding. The OmniACT [11] is a GUI grounding task for Desktop and Web. We derive 6,101 samples in training split and verify on the test split. The accuracy is calculated as whether the predict point correctly locates inside the interest region.

Anomaly Detection. The RealIAD [35] includes real-world, multi-view industrial anomaly. We derive 3,292 training samples and 2,736 test samples, ensuring the two sets are disjoint. We calculated the ROC_AUC.

Medical Image: Skin. The task one of ISIC2018 [4, 10] is lesion segmentation. It includes 2,594 training samples and 1,000 test samples. We measure the bbox_acc metric, which computes the ratio of predicted bounding boxes whose IoU with the ground truth exceeds 0.5.

MathVista. The MathVista-testmini [24] includes 1,000 diverse mathematical and visual tasks. We gather around 10k training data from WeMath [29], MathVision [37], Polymath [8], SceMQA [15], Geometry3K [23].

Implementation Details. We instantialize ViSurf algorithm with Qwen2.5VL-7B [1] and adopt SAM2 [31] if needed. We employ a constant learning rate of 1e-6 for all methods, with a batch size of 32 for SFT and 16 for RLVR and ViSurf. We employ same training steps for fair comparison. For MathVista, the reward function consists of format and accuracy rewards. For other tasks, we adopt the rewards from VisionReasoner [21], which include format accuracy, point accuracy, and bounding box accuracy rewards, etc.

4.2. Comparison of Different Training Paradigms

We compare different post-training paradigms and verify the effectiveness of ViSurf in various domains.

Main Results. A comparative analysis of post-training

Table 3. Employ ViSurf on Qwen2VL-7B.

Method	RealIAD subset		ISIC2018 test
	ROC_AUC	Bbox_Acc	
Baseline	60.0	51.8	
SFT	56.7	94.2	
RLVR	57.1	90.5	
SFT → RLVR	67.5	94.6	
ViSurf	76.0	95.4	

paradigms across various domains is presented in Table 1. Empirical results indicate that ViSurf consistently outperforms existing post-training paradigms across various domains, with an average relative gain of 38.6% over the baseline model. This advantage is particularly significant in domains where the baseline model demonstrates lower competency, such as Non-Object and Anomaly, suggesting the method’s efficacy in addressing domain exceeding model’s knowledge base. However, in domains where the baseline model is already highly proficient, the incremental gains are relatively marginal. We also observe that SFT leads to performance degradation in OmniACT, which may be attributable to potential ‘test data contamination’ during baseline model’s pre-training stage. In comparison, both RLVR and ViSurf preserve the baseline model’s performance. Furthermore, in the case of RealIAD and non-object detection in gRefCOCO, the pure RLVR approach underperforms relative to the original model. We attribute this to the fact that self-generated rollouts frequently produce incorrect answers, thereby hindering model optimization.

Catastrophic Forgetting. We evaluate the performance of ChartQA [26] and DocVQA [27]. As illustrated in Table 2, VQA performance exhibits notable variation across different training paradigms. Both RLVR and ViSurf demonstrate robustness against catastrophic forgetting. In contrast, SFT and SFT → RLVR suffer from performance degradation, which is attributable to catastrophic forgetting.

ViSurf on Other Models. We apply ViSurf to the Qwen2VL-7B [38]. As shown in Table 3, our method consistently outperforms its counterparts. Furthermore, the

Table 4. Ablation of Reward Control Strategy in Section 3.4. ‘Align’: Aligning ground-truth labels with rollouts; ‘Eliminate’: Eliminating thinking format reward for ground-truth labels; ‘Smooth’: Smoothing accuracy reward for ground-truth labels; ‘-’: aligning is not applicable for math.

Align	Eliminate	Smooth	gRefCOCO	ReasonSeg	MathVista
			val	val	testmini
			gIoU	N-Acc	gIoU
✗	✓	✓	59.0	40.2	63.6
✓	✗	✓	72.9	74.1	58.2
✓	✓	✗	61.0	45.7	62.7
✓	✓	✓	66.6	57.1	66.5
					71.6

pure RLVR approach yields the weakest performance on both datasets and even underperforms the baseline on RealiAD, which indicates that external supervision is critical.

4.3. Ablation of Reward Control

Table 4 presents an ablation study of the reward control strategy for ground-truth labels, detailed in Section 3.4.

Aligning Ground-truth Labels with Rollouts Preference. The empirical results underscore the critical importance of this strategy, as its ablation leads to consistent performance degradation across multiple datasets. This observation provides strong empirical validation for the theoretical requirement of $\pi_\theta \approx \pi_{\theta_{old}}$ presented in Equation (10).

Eliminating Thinking Reward for Ground-truth Labels. The results indicate that the reasoning strategy is critical for tasks requiring complex inference, such as those in ReasonSeg and MathVista, as it encourages the model to generate a reasoning process prior to delivering the final answer. Conversely, for the gRefCOCO dataset, where queries are typically limited to simple class types (e.g., “human”) and basic references (e.g., “woman on the right”), omitting the reasoning step yields superior performance. This suggests that the necessity of explicit reasoning is contingent upon the complexity of the underlying task.

Smoothing the Reward for Ground-truth Labels. The performance decline observed across datasets following the ablation of reward smoothing underscores its necessity. Concurrently, the results suggest that the SFT Term in Equation (10) becomes superfluous when the model’s self-rollouts already achieve a higher-quality solution.

4.4. In-depth Analysis

To facilitate a deeper understanding of ViSurf, we provide a detailed analysis of its behavior and properties.

Entropy Analysis During Training. Figure 5 compares the entropy of RLVR, SFT → RLVR and ViSurf. A higher entropy indicates greater exploratory behavior, while lower entropy signifies convergence toward certainty. We observe that ViSurf exhibits an initial entropy drop, indicating the

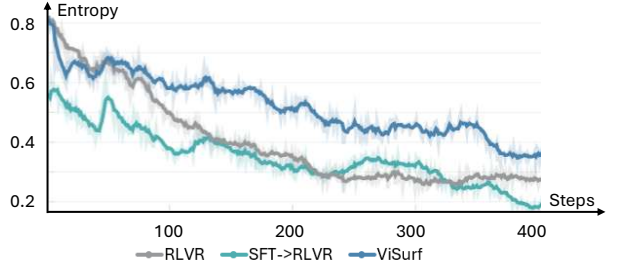


Figure 5. Entropy Analysis of RLVR, SFT → RLVR and ViSurf. ViSurf exhibits an initial drop, then converges slowly.

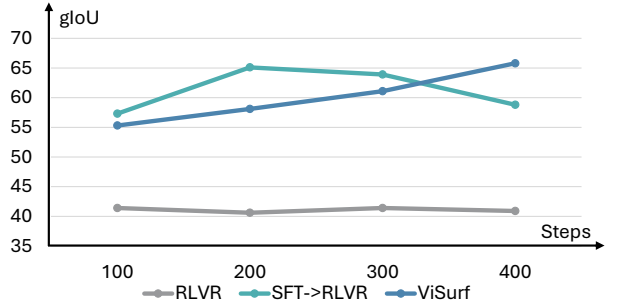


Figure 6. Performance on gRefCOCO in different training steps. ViSurf demonstrates greater stability as training proceeds.

model is fitting the external guidance. Subsequently, ViSurf converges at a slower rate than others, thereby effectively avoiding entropy collapse.

Training Stability. Figure 6 demonstrates that models trained with our method exhibit greater stability than those trained with pure RLVR and SFT → RLVR, as the performance of others decline with longer training. This observation confirms the effectiveness of our approach, indicating that the introduced external guidance acts as a constraint, which stabilizes the training process.

Boundary Analysis. As shown in Table 1, the performance gain of ViSurf is related to the baseline model’s performance. When the baseline performs poorly (e.g., below 50%), indicating its inadequacy for the task, our method yields a substantial improvement. Conversely, when the baseline already achieves high performance (e.g., above 50%), signifying a strong starting point, the upper bound of our method aligns with that of RLVR alone. This observation corroborates our theoretical analysis in Section 3.5.

Reduce the Burden of Prompt Design. The RLVR paradigm relies heavily on explicit instructions to guide the model toward generating rollouts in a specific format, such as *output with format ‘point_2d’*: [2, 3]. In contrast, ViSurf incorporates external guidance with desired format, thereby reducing the dependency on manual prompt engineering. Table 5 compares performance with and without detailed prompts (*details are provided in Section D of the*

Table 5. Comparison of different prompt design. ViSurf achieves satisfying results even without detailed formatting prompt.

Detailed Prompt	ReasonSeg	
	val (gIoU)	test (gIoU)
RLVR	✗ ✓	0.0 66.0
ViSurf	✗ ✓	62.3 66.4
		57.8 65.0

Table 6. Comparison of training cost of different training paradigms with same batch size. Time for two-stage SFT → RLVR is estimated as the addition of SFT and RLVR.

Method	Mem / GPU (G) ↓	Time / Step (s) ↓
SFT	97.7	9.0
RLVR	81.8	22.7
SFT → RLVR	97.9	31.7
ViSurf	81.8	22.9

Table 7. Comparison with SoTAs. ‘-’ means not available.

Method	gRefCOCO		ReasonSeg	
	val	test	val	test
	gIoU	N-Acc	gIoU	gIoU
LISA-7B	61.6	54.7	53.6	48.7
GSVA-7B	66.5	62.4	-	-
SAM4MLLM-7B	69.0	63.0	46.7	-
Qwen2.5VL-7B + SAM2	41.6	3.3	56.9	52.1
SegZero-7B	-	-	62.6	57.5
VisionReasoner-7B	41.5	0.0	66.3	63.6
ViSurf (Qwen2.5VL-7B + SAM2)	72.9	74.1	66.4	65.0

supplementary materials), demonstrating that our approach achieves consistent gains in both settings, whereas RLVR fails without explicit formatting instructions.

Training Cost. We conducted a comparative analysis of the per-step training time for different fine-tuning paradigms. Each method was implemented using well-established frameworks: DeepSpeed [28] and TRL [6] for SFT, and VeRL [33] for RLVR and ViSurf. The results indicate that while RLVR and ViSurf offer greater memory efficiency, they incur a higher computational cost per step, attributable to the overhead of generating rollouts.

4.5. Comparison with State-of-The-Arts

We compare ViSurf against state-of-the-art (SoTA) models on two visual perception tasks: gRefCOCO and ReasonSeg. We compare LISA [12], GSVA [39], SAM4MLLM [2], SegZero [20], VisionReasoner [21]. As shown in Table 7, ViSurf achieves the state-of-the-arts performance on ReasonSeg and gRefCOCO.

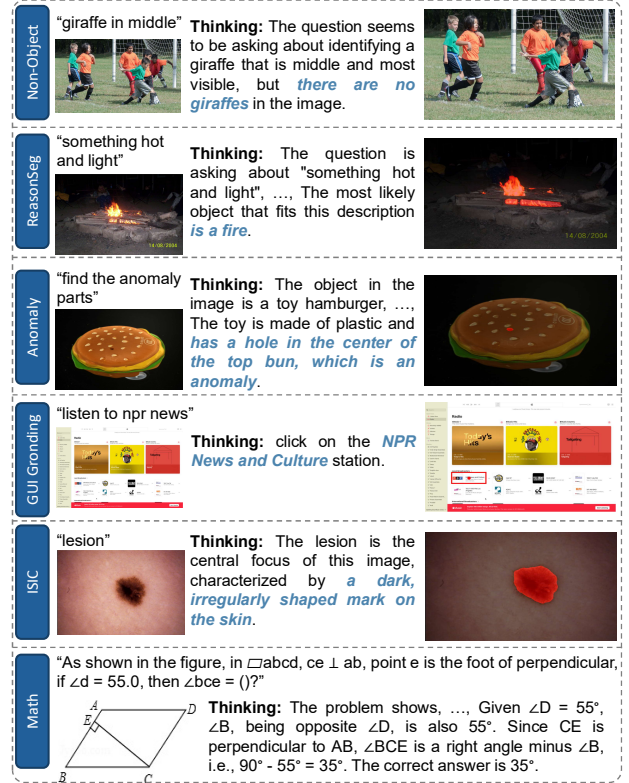


Figure 7. Visualization of ViSurf on various tasks.

4.6. Qualitative Results

Qualitative results on various tasks are presented in Figure 7. The proposed method, ViSurf, successfully localizes normal objects, identifies anomalies, detects non-object cases, and solves mathematical problems.

5. Conclusion

We propose ViSurf, a single-stage post-training paradigm that integrates the benefits of both SFT and RLVR, motivated by a theoretical analysis of their objectives and gradients. The practical implementation of ViSurf involves interleaving ground-truth labels with model-generated rollouts, augmented by three reward control strategies to ensure training stability. Experimental results across diverse benchmarks demonstrate that ViSurf outperforms SFT, RLVR, and a sequential SFT → RLVR pipeline. The subsequent in-depth analysis provides further insights and corroborates the theoretical analysis.

References

- [1] Shuai Bai, Keqin Chen, Xuejing Liu, Jialin Wang, Wenbin Ge, Sibo Song, Kai Dang, Peng Wang, Shijie Wang, Jun Tang, et al. Qwen2. 5-vl technical report. *arXiv preprint arXiv:2502.13923*, 2025. 1, 2, 3, 6

[2] Yi-Chia Chen, Wei-Hua Li, Cheng Sun, Yu-Chiang Frank Wang, and Chu-Song Chen. Sam4mllm: Enhance multi-modal large language model for referring expression segmentation. In *European Conference on Computer Vision*, pages 323–340. Springer, 2024. 8

[3] Zhe Chen, Jiannan Wu, Wenhui Wang, Weijie Su, Guo Chen, Sen Xing, Muyan Zhong, Qinglong Zhang, Xizhou Zhu, Lewei Lu, et al. Internvl: Scaling up vision foundation models and aligning for generic visual-linguistic tasks. In *Proceedings of the IEEE/CVF conference on computer vision and pattern recognition*, pages 24185–24198, 2024. 2

[4] Noel Codella, Veronica Rotemberg, Philipp Tschandl, M Emre Celebi, Stephen Dusza, David Gutman, Brian Helba, Aadi Kalloo, Konstantinos Liopyris, Michael Marchetti, et al. Skin lesion analysis toward melanoma detection 2018: A challenge hosted by the international skin imaging collaboration (isic). *arXiv preprint arXiv:1902.03368*, 2019. 6

[5] Matt Deitke, Christopher Clark, Sangho Lee, Rohun Tripathi, Yue Yang, Jae Sung Park, Mohammadreza Salehi, Niklas Muennighoff, Kyle Lo, Luca Soldaini, et al. Molmo and pixmo: Open weights and open data for state-of-the-art multimodal models. *arXiv e-prints*, pages arXiv–2409, 2024. 2

[6] Hugging Face. TRL - Transformer Reinforcement Learning. <https://github.com/huggingface/trl>, 2024. 8

[7] Daya Guo, Dejian Yang, Haowei Zhang, Junxiao Song, Ruoyu Zhang, Runxin Xu, Qihao Zhu, Shirong Ma, Peiyi Wang, Xiao Bi, et al. Deepseek-r1: Incentivizing reasoning capability in llms via reinforcement learning. *arXiv preprint arXiv:2501.12948*, 2025. 3

[8] Himanshu Gupta, Shreyas Verma, Ujjwala Anantheswaran, Kevin Scaria, Mihir Parmar, Swaroop Mishra, and Chitta Baral. Polymath: A challenging multi-modal mathematical reasoning benchmark. *arXiv preprint arXiv:2410.14702*, 2024. 6

[9] Wenxuan Huang, Bohan Jia, Zijie Zhai, Shaosheng Cao, Zheyu Ye, Fei Zhao, Zhe Xu, Yao Hu, and Shaohui Lin. Vision-r1: Incentivizing reasoning capability in multimodal large language models. *arXiv preprint arXiv:2503.06749*, 2025. 2

[10] International Skin Imaging Collaboration (ISIC). Isic 2018: Skin lesion analysis towards melanoma detection. <https://challenge.isic-archive.com/data/#2018>, 2018. 6

[11] Raghav Kapoor, Yash Parag Butala, Melisa Russak, Jing Yu Koh, Kiran Kamble, Waseem AlShikh, and Ruslan Salakhutdinov. Omniact: A dataset and benchmark for enabling multimodal generalist autonomous agents for desktop and web. In *European Conference on Computer Vision*, pages 161–178. Springer, 2024. 6

[12] Xin Lai, Zhuotao Tian, Yukang Chen, Yanwei Li, Yuhui Yuan, Shu Liu, and Jiaya Jia. Lisa: Reasoning segmentation via large language model. In *Proceedings of the IEEE/CVF Conference on Computer Vision and Pattern Recognition*, pages 9579–9589, 2024. 5, 8

[13] Bo Li, Yuanhan Zhang, Dong Guo, Renrui Zhang, Feng Li, Hao Zhang, Kaichen Zhang, Peiyuan Zhang, Yanwei Li, Zi-wei Liu, et al. Llava-onevision: Easy visual task transfer. *arXiv preprint arXiv:2408.03326*, 2024. 2

[14] Yanwei Li, Yuechen Zhang, Chengyao Wang, Zhisheng Zhong, Yixin Chen, Ruihang Chu, Shaoteng Liu, and Jiaya Jia. Mini-gemini: Mining the potential of multi-modality vision language models. *arXiv preprint arXiv:2403.18814*, 2024. 2

[15] Zhenwen Liang, Kehan Guo, Gang Liu, Taicheng Guo, Yujun Zhou, Tianyu Yang, Jiajun Jiao, Renjie Pi, Jipeng Zhang, and Xiangliang Zhang. Scemqa: A scientific college entrance level multimodal question answering benchmark. *arXiv preprint arXiv:2402.05138*, 2024. 6

[16] Chang Liu, Henghui Ding, and Xudong Jiang. Gres: Generalized referring expression segmentation. In *Proceedings of the IEEE/CVF conference on computer vision and pattern recognition*, pages 23592–23601, 2023. 3, 5

[17] Haotian Liu, Chunyuan Li, Qingyang Wu, and Yong Jae Lee. Visual instruction tuning. *Advances in neural information processing systems*, 36:34892–34916, 2023. 1, 2

[18] Haotian Liu, Chunyuan Li, Yuheng Li, and Yong Jae Lee. Improved baselines with visual instruction tuning. In *Proceedings of the IEEE/CVF conference on computer vision and pattern recognition*, pages 26296–26306, 2024. 2

[19] Jiazheng Liu, Yuchuan Deng, and Long Chen. Empowering small vlms to think with dynamic memorization and exploration. *arXiv preprint arXiv:2506.23061*, 2025. 2

[20] Yuqi Liu, Bohao Peng, Zhisheng Zhong, Zihao Yue, Fanbin Lu, Bei Yu, and Jiaya Jia. Seg-zero: Reasoning-chain guided segmentation via cognitive reinforcement. *arXiv preprint arXiv:2503.06520*, 2025. 1, 2, 3, 8

[21] Yuqi Liu, Tianyuan Qu, Zhisheng Zhong, Bohao Peng, Shu Liu, Bei Yu, and Jiaya Jia. Visionreasoner: Unified visual perception and reasoning via reinforcement learning. *arXiv preprint arXiv:2505.12081*, 2025. 1, 2, 3, 5, 6, 8

[22] Ziyu Liu, Zeyi Sun, Yuhang Zang, Xiaoyi Dong, Yuhang Cao, Haodong Duan, Dahua Lin, and Jiaqi Wang. Visual-rft: Visual reinforcement fine-tuning. *arXiv preprint arXiv:2503.01785*, 2025. 2

[23] Pan Lu, Ran Gong, Shibiao Jiang, Liang Qiu, Siyuan Huang, Xiaodan Liang, and Song-Chun Zhu. Inter-gps: Interpretable geometry problem solving with formal language and symbolic reasoning. *arXiv preprint arXiv:2105.04165*, 2021. 6

[24] Pan Lu, Hritik Bansal, Tony Xia, Jiacheng Liu, Chunyuan Li, Hannaneh Hajishirzi, Hao Cheng, Kai-Wei Chang, Michel Galley, and Jianfeng Gao. Mathvista: Evaluating mathematical reasoning of foundation models in visual contexts. *arXiv preprint arXiv:2310.02255*, 2023. 6

[25] Lu Ma, Hao Liang, Meiyi Qiang, Lexiang Tang, Xiaochen Ma, Zhen Hao Wong, Junbo Niu, Chengyu Shen, Runming He, Bin Cui, et al. Learning what reinforcement learning can't: Interleaved online fine-tuning for hardest questions. *arXiv preprint arXiv:2506.07527*, 2025. 2

[26] Ahmed Masry, Do Xuan Long, Jia Qing Tan, Shafiq Joty, and Enamul Hoque. Chartqa: A benchmark for question answering about charts with visual and logical reasoning. *arXiv preprint arXiv:2203.10244*, 2022. 6

[27] Minesh Mathew, Dimosthenis Karatzas, and CV Jawahar. Docvqa: A dataset for vqa on document images. In *Proceedings of the IEEE/CVF winter conference on applications of computer vision*, pages 2200–2209, 2021. 6

[28] Microsoft and DeepSpeed Team. DeepSpeed. <https://github.com/deepspeedai/DeepSpeed>, 2020. 8

[29] Runqi Qiao, Qiuna Tan, Guanting Dong, Minhui Wu, Chong Sun, Xiaoshuai Song, Zhuoma GongQue, Shanglin Lei, Zhe Wei, MiaoXuan Zhang, et al. We-math: Does your large multimodal model achieve human-like mathematical reasoning? *arXiv preprint arXiv:2407.01284*, 2024. 6

[30] Rafael RafaIlov, Archit Sharma, Eric Mitchell, Christopher D Manning, Stefano Ermon, and Chelsea Finn. Direct preference optimization: Your language model is secretly a reward model. *Advances in neural information processing systems*, 36:53728–53741, 2023. 2

[31] Nikhila Ravi, Valentin Gabeur, Yuan-Ting Hu, Ronghang Hu, Chaitanya Ryali, Tengyu Ma, Haitham Khedr, Roman Rädl, Chloe Rolland, Laura Gustafson, et al. Sam 2: Segment anything in images and videos. *arXiv preprint arXiv:2408.00714*, 2024. 3, 6

[32] John Schulman, Filip Wolski, Prafulla Dhariwal, Alec Radford, and Oleg Klimov. Proximal policy optimization algorithms. *arXiv preprint arXiv:1707.06347*, 2017. 2

[33] ByteDance Seed. verl: Volcano Engine Reinforcement Learning for LLMs. <https://github.com/volcengine/verl>, 2024. 8

[34] Zhihong Shao, Peiyi Wang, Qihao Zhu, Runxin Xu, Junxiao Song, Xiao Bi, Haowei Zhang, Mingchuan Zhang, YK Li, Yang Wu, et al. Deepseekmath: Pushing the limits of mathematical reasoning in open language models. *arXiv preprint arXiv:2402.03300*, 2024. 1, 2, 3

[35] Chengjie Wang, Wenbing Zhu, Bin-Bin Gao, Zhenye Gan, Jiangning Zhang, Zhihao Gu, Shuguang Qian, Mingang Chen, and Lizhuang Ma. Real-iad: A real-world multi-view dataset for benchmarking versatile industrial anomaly detection. In *Proceedings of the IEEE/CVF Conference on Computer Vision and Pattern Recognition*, pages 22883–22892, 2024. 6

[36] Chengyao Wang, Zhisheng Zhong, Bohao Peng, Senqiao Yang, Yuqi Liu, Haokun Gui, Bin Xia, Jingyao Li, Bei Yu, and Jiaya Jia. Mgm-omni: Scaling omni llms to personalized long-horizon speech. *arXiv preprint arXiv:2509.25131*, 2025. 2

[37] Ke Wang, Junting Pan, Weikang Shi, Zimu Lu, Houxing Ren, Aojun Zhou, Mingjie Zhan, and Hongsheng Li. Measuring multimodal mathematical reasoning with math-vision dataset. *Advances in Neural Information Processing Systems*, 37:95095–95169, 2024. 6

[38] Peng Wang, Shuai Bai, Sinan Tan, Shijie Wang, Zhihao Fan, Jinze Bai, Keqin Chen, Xuejing Liu, Jialin Wang, Wenbin Ge, et al. Qwen2-vl: Enhancing vision-language model’s perception of the world at any resolution. *arXiv preprint arXiv:2409.12191*, 2024. 1, 2, 6

[39] Zhuofan Xia, Dongchen Han, Yizeng Han, Xuran Pan, Shiji Song, and Gao Huang. Gsva: Generalized segmentation via multimodal large language models. In *Proceedings of the IEEE/CVF Conference on Computer Vision and Pattern Recognition*, pages 3858–3869, 2024. 8

[40] Zhenhua Xu, Yan Bai, Yujia Zhang, Zhuoling Li, Fei Xia, Kwan-Yee K Wong, Jianqiang Wang, and Hengshuang Zhao. Drivegpt4-v2: Harnessing large language model capabilities for enhanced closed-loop autonomous driving. In *Proceedings of the Computer Vision and Pattern Recognition Conference*, pages 17261–17270, 2025. 2

[41] Zhiyuan You, Xin Cai, Jinjin Gu, Tianfan Xue, and Chao Dong. Teaching large language models to regress accurate image quality scores using score distribution. In *Proceedings of the Computer Vision and Pattern Recognition Conference*, pages 14483–14494, 2025. 2

[42] Qiying Yu, Zheng Zhang, Ruofei Zhu, Yufeng Yuan, Xiaochen Zuo, Yu Yue, Tiantian Fan, Gaohong Liu, Lingjun Liu, Xin Liu, et al. Dapo: An open-source llm reinforcement learning system at scale, 2025. URL <https://arxiv.org/abs/2503.14476>, 2025. 1, 2

[43] Wenhao Zhang, Yuexiang Xie, Yuchang Sun, Yanxi Chen, Guoyin Wang, Yaliang Li, Bolin Ding, and Jingren Zhou. On-policy rl meets off-policy experts: Harmonizing supervised fine-tuning and reinforcement learning via dynamic weighting. *arXiv preprint arXiv:2508.11408*, 2025. 2

[44] Zhisheng Zhong, Chengyao Wang, Yuqi Liu, Senqiao Yang, Longxiang Tang, Yuechen Zhang, Jingyao Li, Tianyuan Qu, Yanwei Li, Yukang Chen, et al. Lyra: An efficient and speech-centric framework for omni-cognition. *arXiv preprint arXiv:2412.09501*, 2024. 2

ViSurf: Visual Supervised-and-Reinforcement Fine-Tuning for Large Vision-and-Language Models

Supplementary Material

A. Discussion and Future Work

The principal insight of ViSurf is the effective combination of RLVR’s internal reinforcement and the external guidance of SFT. Although the ground-truth labels in this work are limited to final answers, our ViSurf paradigm is inherently compatible to incorporate explicit reasoning traces. The flexibility also ensures compatibility with advanced techniques like knowledge distillation, where reasoning traces from larger models could be directly incorporated. We anticipate that this work will provide a foundation for future research in LVLMs’ post-training.

B. Additional Explanation on pure RLVR

The performance of pure RLVR is heavily influenced by randomness. In approximately one out of ten runs, the old policy model $\pi_{\theta_{old}}$ can generate correct non-object outputs in the initial steps, thereby achieving competitive performance (see Table 8), yet still marginally inferior to ViSurf.

Table 8. Comparison under different training paradigms.

Method	gRefCOCO	
	gIoU	val
Baseline	33.4	1.8
SFT	41.6	3.3
RLVR (90% runs)	42.8	0.0
RLVR (10% runs)	62.9	49.3
SFT → RLVR	58.6	38.1
ViSurf	66.6	57.1

C. Non Object Training Data

The training data for gRefCOCO was adapted from the VisionReasoner training data [21], from which we utilized 7k referring expression samples. To enhance the model’s ability to handle cases where no target object is present, we augmented this dataset with 200 non-object examples. These negative samples were generated by providing a question that is unanswerable given the image content and training the model to output an empty list (<answer>[]</answer>).

D. Illustration of Prompt Design

Table 9 shows prompt with detailed format instruction, where we provide desired output format for model. Table 10 shows prompt without detailed format instruction, where we simply write ‘answer here’ between answer tags.

Table 9. Prompt **with** detailed format instruction. We provide detailed format instructions between answer tags.

Prompt with Detailed Instruction
<p>"Please find “{<i>Question</i>}” with bboxes and points." "Compare the difference between object(s) and find the most closely matched object(s)." "Output the thinking process in <think> </think> and final answer in <answer> </answer> tags." "Output the bbox(es) and point(s) inside the interested object(s) in JSON format." i.e. <think> thinking process here </think> <answer>[{"bbox_2d": [10, 100, 200, 210], "point_2d": [30, 110]}, {"bbox_2d": [225, 296, 706, 786], "point_2d": [302, 410]}]</answer></p>

Table 10. Prompt **without** Detailed Instruction. We do not provide detailed format instructions between answer tags.

Prompt without Detailed Instruction
<p>"Please find “{<i>Question</i>}” with bboxes and points." "Compare the difference between object(s) and find the most closely matched object(s)." "Output the thinking process in <think> </think> and final answer in <answer> </answer> tags." "Output the bbox(es) and point(s) inside the interested object(s) in JSON format." i.e. <think> thinking process here </think> <answer> answer here </answer></p>